



Pergamon

Acta Materialia 50 (2002) 4021–4035



www.actamat-journals.com

Precipitation strengthening at ambient and elevated temperatures of heat-treatable Al(Sc) alloys

David N. Seidman *, Emmanuelle A. Marquis, David C. Dunand

Department of Material Science and Engineering, Northwestern University, Evanston, IL, 60208, USA

Received 15 January 2002; accepted 24 May 2002

Abstract

Yield strength at ambient temperature and creep resistance between 225 and 300°C were investigated in dilute Al(Sc) alloys containing coherent Al₃Sc precipitates, which were grown by heat-treatments to radii in the range 1.4–9.6 nm. The dependence of the ambient-temperature yield stress on precipitate size is explained using classical precipitation strengthening theory, which predicts a transition from precipitate shearing to Orowan dislocation looping mechanisms at a precipitate radius of 2.1 nm, in good agreement with experimental data. At 300°C creep threshold stresses are observed and found to be much lower than the yield stresses, indicative of a climb-controlled bypass mechanism. The threshold stress increases with increasing precipitate radius, in qualitative agreement with a climb model taking into account stiffness and lattice mismatches between matrix and precipitates [1]. © 2002 Acta Materialia Inc. Published by Elsevier Science Ltd. All rights reserved.

Keywords: Aluminum alloys; Scandium; Mechanical properties; Precipitation strengthening; Creep; Threshold stress

1. Introduction

Aluminum alloyed with scandium has excellent mechanical properties at room temperature, due to the presence of coherent, nanometer size Al₃Sc precipitates that can be obtained at a very high number density, thus blocking mobile dislocations and stabilizing a fine-grain structure [2]. These Al₃Sc precipitates are stable against coarsening up

to temperatures of 350°C [3], much higher than the capabilities of commercial age-hardening 2xxx and 6xxx series alloys containing Cu, Mg and Si, whose microstructures coarsen rapidly above 250°C [4]. Scandium-containing aluminum alloys thus constitute castable, heat-treatable, precipitation-strengthened alloys that can be used at temperatures significantly higher than conventional aluminum alloys.

Precipitation strengthening at room temperature can occur by means of two mechanisms, depending on the precipitate size. First, the shearing mechanism for small precipitates involves chemical, coherency, modulus mismatch, and anti-phase boundary (APB) strengthening [5]. Second, the

* Corresponding author. Tel.: +1 847 491 4391.

E-mail address: d-seidman@northwestern.edu (D>N> Seidman) (D.N. Seidman).

Orowan bypass process, where dislocation looping around precipitates, is active for larger precipitates [5]. Relatively little information exists in the literature on the deformation mechanisms of Al(Sc) alloys. Taking into account both lattice parameter mismatch strains and the APB energy, Parker [6] concluded that the experimental room-temperature yield strength of Al(Sc) alloys, containing low volume fractions of Al_3Sc precipitates, is well described by the sum of the theoretical coherency and order strengthening contributions, i.e., precipitate shearing is the operational mechanism. Miura et al. [7] proposed that the tensile deformation properties between 25 and 250°C of an overaged Al-0.23 wt.% Sc alloy, containing precipitates with an average radius of 7.9 nm, occurs by Orowan dislocation looping and/or dislocation climb at the particles. Torma et al. [8] concluded that the Orowan dislocation mechanism operates at room temperature in Al-0.18 and 0.31 wt.% Sc alloys for precipitate radii larger than 4.3 nm. At elevated temperature, most studies report that Al(Sc) alloys have good superplastic properties [9,10] because the stable Al_3Sc precipitates stabilize very fine grain sizes, which leads to rapid diffusional creep. Only one study concerned itself with coarse-grained Al(Sc) alloys, where the creep behavior of two Al(Sc) alloys containing low volume fractions of Al_3Sc precipitates was investigated and threshold stresses for creep at 300°C were measured [11].

This article reports on a systematic study of the yield and creep behavior, as well as the corresponding dislocation mechanisms, in aluminum alloys containing low volume-fractions of Al_3Sc precipitates (less than 0.74 vol.%) at room temperature and between 225 and 300°C, i.e., at homologous temperatures, T/T_m , between 0.50 and 0.64 (where T_m is the absolute melting temperature of aluminum). The alloys studied are coarse-grained, so that creep is controlled by dislocation mechanisms, rather than by grain-boundary sliding, as in fine-grained super-plastic alloys [9,10]. This study aims at identifying the governing mechanisms for the strength of precipitation-strengthened alloys at ambient and high temperatures, which will be used for future Al(Sc) alloy design.

2. Experimental procedures

2.1. Materials preparation and heat-treatments

Billets of aluminum with 0.10, 0.15, 0.20 or 0.30 wt.% Sc were prepared by melting in air appropriate amounts of 99.9 wt.% pure Al and an Al-1.2 wt.% Sc master alloy, followed by casting into a graphite mold. The chemical composition was verified for each casting (Galbraith Laboratories Inc., Knoxville, TN). Heat-treatments consisted of homogenization in air at 648°C for 24 h, water-quenching to room temperature, and aging in air at temperatures between 275–400°C for times between 10 min and 100 hours, which was terminated by water quenching. Aging was performed within 24 h after quenching. Some of the samples underwent double aging treatments, e.g., aging at 300°C for 5 h, water quenching, and then aging at 400°C for times between 1 and 10 h, followed by room-temperature water-quenching.

2.2. Mechanical properties

Vickers microhardness was measured on polished samples using the average value of 20 independent measurements made on several grains. Room-temperature compression tests were performed on the Al-0.3 wt.% Sc alloy to measure its yield strength. The $4 \times 4 \times 8 \text{ mm}^3$ parallelepiped specimens were deformed in a compression cage at constant cross-head speeds corresponding to strain rates of about 0.03 s^{-1} . Tensile tests were performed in air at 300°C on the Al-0.15 wt.% Sc alloy at a deformation rate of 0.03 s^{-1} , using a water-cooled extensometer placed on the gauge length. Creep specimens with a cylindrical gauge diameter of 4 mm and length of 20 mm were machined from the cast alloys. Tensile creep tests were performed in air under constant load corresponding to stresses in the range 5–50 MPa, and at constant temperature (225–300°C). Gauge length elongation was measured utilizing a high-temperature extensometer connected to a linear variable differential transducer. After steady-state deformation was achieved, the load was increased, resulting in three to five data points for each specimen.

2.3. Microstructural observations

Samples were polished with diamond paste down to 0.3 μm and etched with Keller's etchant to reveal the grain structure. The absence of primary precipitates was checked by scanning electron microscopy on polished cross sections. Conventional transmission electron microscopy (TEM) was performed on an Hitachi 8100 operating at 200 kV using a double-tilt stage. TEM was performed both before and after heat-treatment to determine precipitate radius, morphologies, and interface coherency, as well as the dislocation structures. Precipitate size distributions were measured by image analysis of TEM micrographs. A minimum of 100 precipitates was analyzed for each heat-treatment. Some of the creep experiments were interrupted in the steady-state regime by cooling rapidly under load to room temperature, in order to maintain the dislocation structure developed during creep. Slices, 350 μm in thickness, were cut from the creep specimen gauge lengths perpendicular to the direction of the applied load. The slices were mechanically polished to a thickness of 200 μm , and twinjet electro-polished with a solution of 5% perchloric acid in methanol at -30°C .

3. Results

3.1. Initial microstructure

The cast and annealed alloys are coarse-grained, with an equiaxed grain size of 1–2 mm, independent of scandium concentration. No subgrains were observed by TEM in the microstructure of the alloys before creep deformation. A high number density of nearly spherical Al_3Sc precipitates was formed as a result of all the aging treatments. These precipitates are coherent with the Al matrix, as coherency strain (Ashby–Brown contrast) was visible and no interfacial dislocations were observed. Representative TEM micrographs (Figs. 1a and 1b) show the effect of temperature on the precipitate number density and size for the Al-0.3 wt.% Sc alloy. For a constant aging time, as the aging temperature increases, the average precipitate radius increases and the number density of pre-

cipitates decreases. The effect of composition is illustrated by Figs. 1a and 1c, which demonstrate a decreasing number density (by a factor of about 200) and increasing precipitate radius (1.4 nm–9 nm), when the scandium concentration is decreased from 0.3 to 0.1 wt.% Sc for the same aging conditions. The strain-field contrast due to coherent interfaces is illustrated in Fig. 1d. Fig. 2 shows precipitate size distribution functions for the Al-0.3 wt.% Sc alloy, after various heat-treatments, which are reasonably close to predictions given by the Lifshitz-Slyozov-Wagner (LSW) theory, as modified by Ardell [12–14].

When aging the Al-0.3 wt.% Sc alloy at 400°C , precipitate-free zones (PFZs) were observed near grain boundaries on which large incoherent precipitates form, as shown in Fig. 3. Because these PFZs are detrimental to the mechanical properties of Al alloys [15], double-aging treatments, (e.g., 300°C for 5 h followed by 3–10 h at 400°C), were used to limit the amount of grain boundary precipitation in creep samples. Precipitates nucleate within the grains during the first aging treatment at 300°C and coarsen during the subsequent aging treatment at 400°C .

3.2. Room-temperature mechanical properties

The aging response of the alloys, measured from changes in Vickers microhardness, exhibits four different regions (Figs. 4 and 5): (a) an incubation period; (b) a short transient period with a rapid increase in hardness values; (c) a plateau at high hardness values (peak aging); and (d) a slow decrease of the hardness. The temperature dependence of hardness evolution is shown in Fig. 4 for an Al-0.3 wt.% Sc alloy. As the aging temperature increases from 275 – 400°C , the incubation time decreases, the time to reach peak hardness decreases, and the rate of hardness drop after peak aging increases (as observed at 350 and 400°C). The dependence of hardness on scandium concentration was measured by aging Al-0.1, 0.2 and 0.3 wt.% Sc alloys at 300°C as shown in Fig. 5. As the scandium concentration increases, the incubation time decreases and the value of peak hardness increases. As seen from the hardness curves of Fig. 5, the time span of the peak hardness pla-

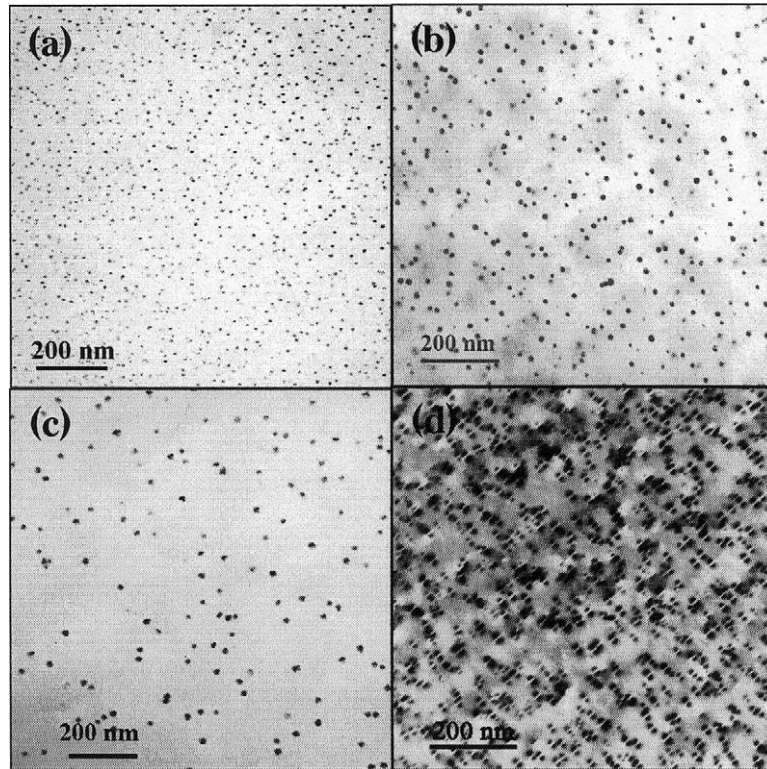


Fig. 1. Dark-field TEM micrographs: (a) Al-0.3 wt.% Sc alloy aged at 300°C for 72 h; (b) Al-0.3 wt.% Sc alloy aged at 400°C for 5 h; (c) Al-0.1 wt.% Sc alloy aged at 300°C for 72 h; and (d) coherency strain contrast in the Al-0.2 wt.% Sc alloy aged at 300°C for 72 h (a–c) using the (100) reflection and (d) employs a two-beam condition using the (200) reflection.

teau for aging at 300°C is longer than that of a creep experiment, so the creep tests performed at 300°C and below can safely be considered not to alter the precipitate size distribution of the alloys.

The yield strength at room temperature of an Al-0.3 wt.% Sc alloy aged at 300°C for 5 h is 209 ± 10 MPa (average value for two tests). After a subsequent anneal at 400°C for 7 h, the yield strength decreases to 140 ± 10 MPa. These values constitute a significant improvement when compared to 99.6% pure Al in the O-temper (annealed) state, which has a tensile yield strength of 30 MPa [16].

3.3. High-temperature mechanical properties

At 300°C and a deformation rate of 0.03 s^{-1} , a yield strength of 101 MPa is measured for an Al-0.15 wt.% Sc alloy aged at 300°C for 5 h and 400°C for 1 h. When aging at 400°C was increased

to 3 and 7 h, the yield strength at 300°C decreases to 70 and 57 MPa, respectively.

A normal primary creep region, where the strain rate decreases continuously, always precedes the steady-state creep regime. All specimens that were deformed to fracture, at different stress levels exhibited more than 10% strain, with the exception of the Al-0.3 wt.% Sc alloy directly aged at 400°C after quenching from the homogenization temperature, which showed only 4% plastic deformation and brittle-like fracture along grain boundaries. Despite the low scandium concentration levels, all alloys exhibit significant improvements in creep resistance at 300°C as compared to pure aluminum (Fig. 6). In the experimental range of strain rates (3×10^{-9} to $3 \times 10^{-4} \text{ s}^{-1}$), high stress exponents were measured, decreasing from $n = 24\text{--}30$ at strain rates below 10^{-7} s^{-1} , to $n = 9\text{--}14$ at higher strain rates (Fig. 6). At even higher strain rates,

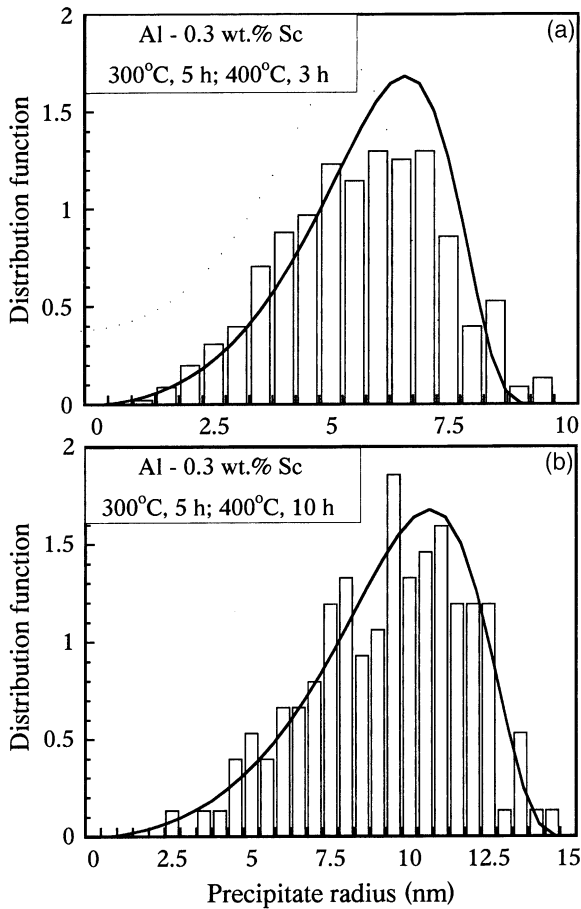


Fig. 2. Precipitate size distributions for the Al-0.3 wt.% Sc alloy for two different heat-treatments. The theoretical LSW distribution function, as modified by Ardell [14] to correct for the volume fraction, is shown as a solid line for comparison.

which were not investigated in this study, it is anticipated that the behavior of the precipitate-strengthened alloy should converge to the behavior of the pure material and the stress exponents should decrease to values of 4–5. Two of the alloys (Al-0.3 wt.% Sc and Al-0.2 wt.% Sc) were tested at various temperatures between 225 and 300°C as displayed in Fig. 7. The same peak aging treatment (300°C for 5 h) was used for all specimens. Both the stress exponents and activation energies are high, the latter varying from 230 to 320 kJ mol⁻¹. Finally, the Al-0.3 wt.% Sc alloy was creep-tested at 300°C after various heat-treatments between 300 and 400°C, providing a range

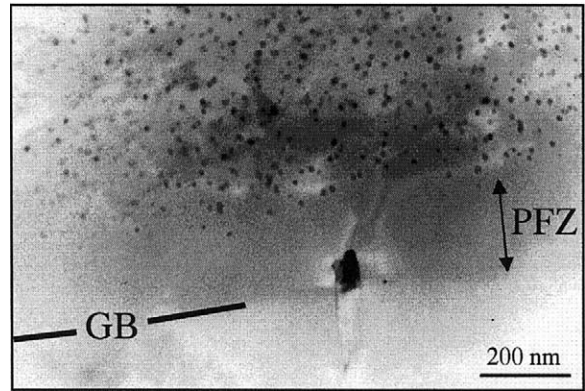


Fig. 3. Dark-field TEM image of a precipitate-free zone (PFZ) at a grain boundary (GB) in an Al-0.3 wt.% Sc alloy aged at 400°C for 5 h. A large incoherent precipitate is also visible at the grain boundary.

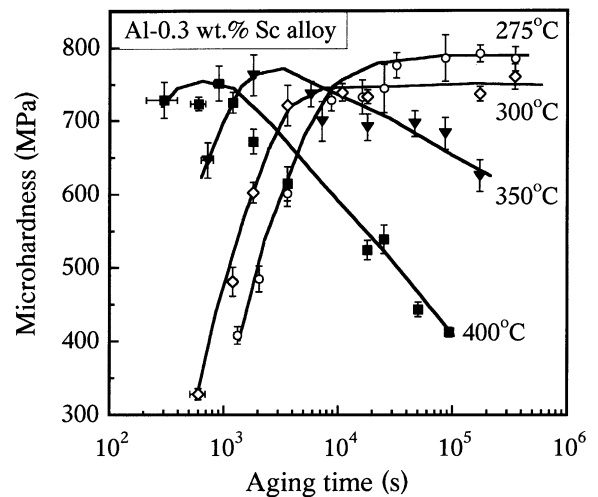


Fig. 4. Vickers micro-hardness versus aging time for an Al-0.3 wt.% Sc alloy as a function of aging temperatures (275, 300, 350 and 400 °C).

of precipitate radii [3] at constant volume fraction. As shown in Fig. 8, the creep resistance increases with increasing precipitate radius in the range 1.4–7.8 nm.

3.4. Deformed microstructure

Fig. 9(a,b) show dislocation structures for an Al-0.3 wt.% Sc alloy deformed to 20% in compression at room temperature. For an average precipitate

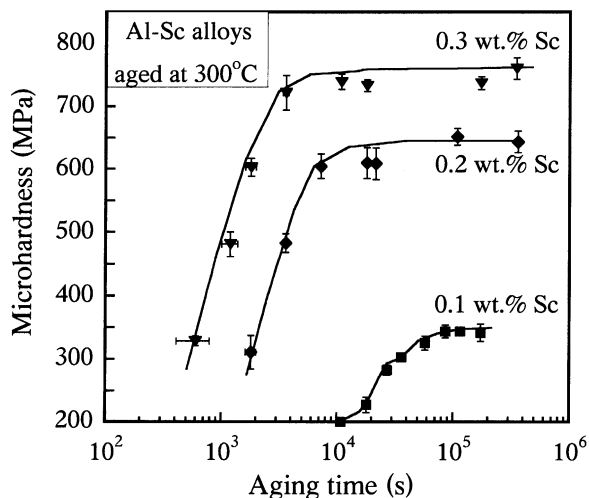


Fig. 5. Vickers micro-hardness versus aging time at 300°C as a function of Sc concentration (0.1, 0.2 and 0.3 wt.%).

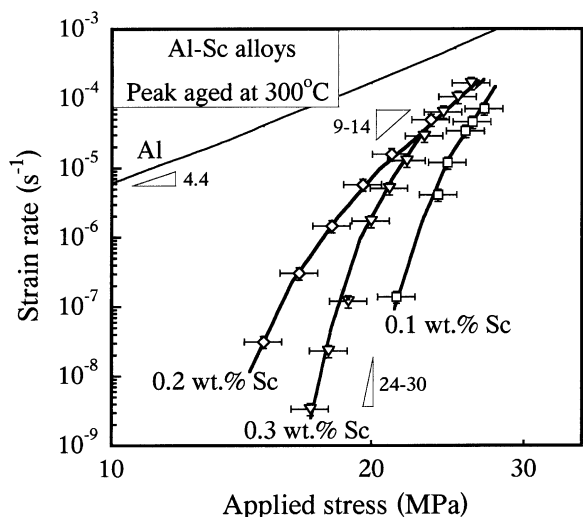


Fig. 6. Steady-state strain-rate at 300°C versus applied stress as a function of Sc concentration (0.1, 0.2 and 0.3 wt.%) for alloys peak-aged at 300°C (24 h, 6 h, 6 h respectively). Data for pure aluminum with a stress exponent $n=4.4$ is plotted for comparison, using the available creep parameters from Ref. [33].

radius of 1.4 nm resulting from aging at 300°C for 5 h, pairs of dislocations are observed (Fig. 9(a)). The average spacing of the dislocations in a pair is approximately 14 nm. Fig. 9(b) shows the dislocation structure present in the same alloy, aged at

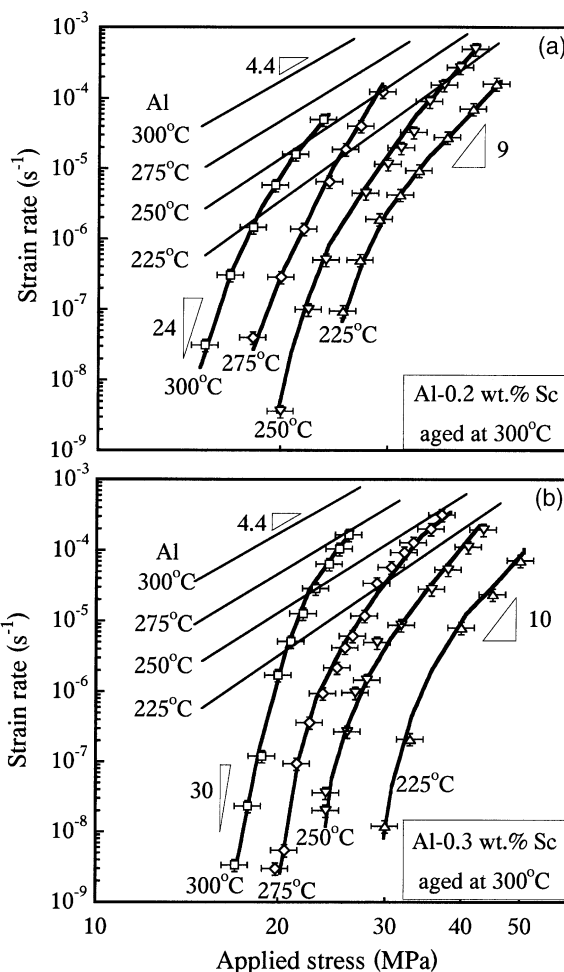


Fig. 7. Effect of test temperature on steady-state creep behavior: (a) Al-0.2 wt.% Sc; and (b) Al-0.3 wt.% Sc. Both alloys were peak-aged at 300°C for 6 h. Data for pure Al is from Ref. [33].

400°C for 3 h following the above 300°C treatment, where the average precipitate radius is 5.9 nm. Dislocation loops are observed around some Al_3Sc precipitates and no dislocation pairs are visible.

In all deformed creep specimens, dislocations pinned at Al_3Sc precipitates could be seen by TEM, suggesting strong dislocation-precipitate interactions. Different crept microstructures were observed, depending on the average precipitate size. As seen in Fig. 10(a), dislocation walls separate subgrains with a low dislocation density for

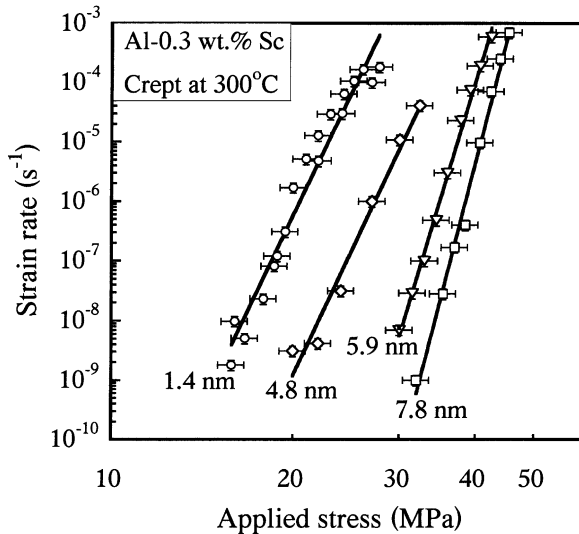


Fig. 8. Steady-state strain rate at 300°C versus applied stress for the Al-0.3 wt.% Sc alloy containing precipitates of average radii ranging from 1.4 nm to 7.8 nm. Data for pure Al is from Ref. [33].

small precipitates of average radius 1.4 nm. No subgrains are observed but a uniform distribution of tangled dislocations and dislocations pinned at precipitates are present for larger precipitates of average radius 7.8 nm (Fig. 10(b)).

4. Discussion

4.1. Microstructure

The aging treatments produce Al_3Sc precipitates by decomposition of the supersaturated $\text{Al}(\text{Sc})$ solid-solutions [2,3]. The precipitates have the L1_2 structure as reported by Ref. [4] and the state of coherency of the precipitate/matrix interface (Fig. 1d) is explained by the low lattice parameter mismatch between the Al_3Sc precipitates and the matrix [3]. The precipitate radius increases with increasing annealing time, as a result of coarsening. For equal aging times, the average precipitate radius also increases with aging temperature due to a decreasing number density of precipitates and faster diffusion of Sc in Al [3]. The precipitate radius distribution follows the predictions of LSW theory as shown in Fig. 2; similar behavior has been reported in [3]. Also, the measured distributions agree with previous microstructural study [3,17] for similar Sc composition ranges. The faceting of the Al_3Sc precipitates, as previously observed by high-resolution TEM [3], is modest enough that the precipitate shapes in the present study are well approximated by spheroids. Whereas the Al_3Sc precipitates remain coherent for the heat-treatments used, the presence of PFZs after aging at 400°C indicates that heterogeneous

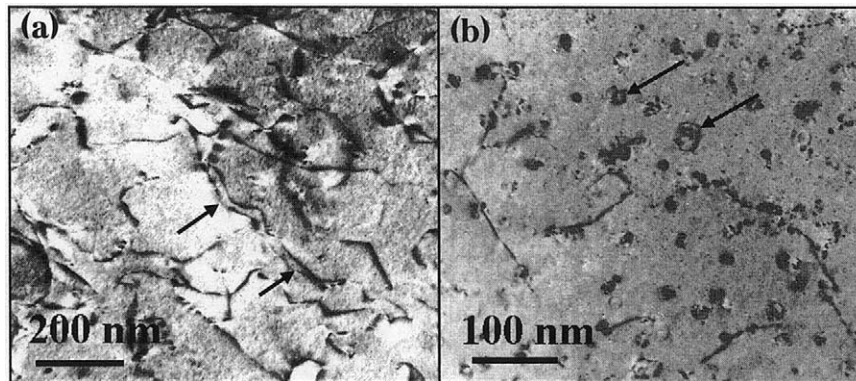


Fig. 9. TEM micrographs of: (a) dislocation structure after ambient temperature compression to 20% strain for an Al-0.3 wt.% Sc alloy aged at 300°C for 5 h with fine precipitates ($r=1.4$ nm)—pairs of dislocations are marked with arrows; and (b) same alloy aged at 300°C for 5 h and at 400°C for 3 h with coarser precipitates ($r=5.9$ nm)—dislocation loops around precipitates are marked with arrows.

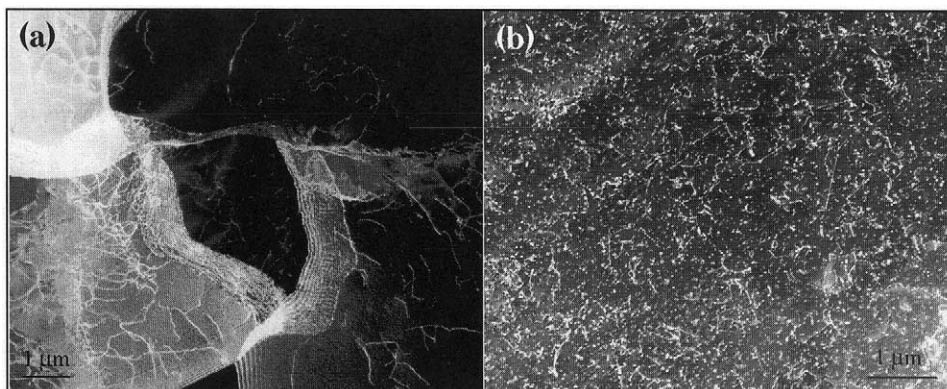


Fig. 10. TEM micrographs of post-creep dislocation structures: (a) Al-0.3 wt.% Sc alloy aged at 300°C for 5 h, crept at 300°C under 22 MPa showing subgrain walls; and (b) Al-0.3 wt.% Sc alloy aged at 300°C for 5 h and 400°C for 7 h and then crept at 300°C under 36 MPa, exhibiting no subgrain structure.

nucleation at grain boundaries becomes more important as the aging temperature increases at constant Sc concentration, because the homogeneous nucleation current decreases due to the lower Sc supersaturation at a higher temperature. As observed in Al(Li) alloys [18], heterogeneous nucleation at grain boundaries is then favored and PFZs are formed near grain boundaries as solute atoms diffuse to the grain boundary precipitates.

After deformation at room temperature, two different dislocation structures are observed. The dislocation pairs present in the alloy containing the smallest precipitate radii (Fig. 9(a)) suggest a shearing mechanism. As observed in Al(Li) alloys with coherent $L1_2$ Al_3Li precipitates [19], dislocations tend to travel in pairs because shearing of the $L1_2$ precipitates by a pair of matrix dislocations with a Burgers vector of the type $a/2\langle 110 \rangle$ restores perfect order of the precipitate on $\{111\}$ -type slip planes. The dislocation loops present around the precipitates of larger radius (Fig. 9(b)) indicate operation of the Orowan dislocation bypass mechanism.

After creep deformation, formation of subgrains is observed for the Al-0.3 wt.% Sc alloys containing small precipitates of radius 1.4 nm, after aging at 300°C for 6 h, as shown in Fig. 10(a). Dislocation climb over nanometer-size precipitates is expected to be rapid, so the deformed microstructure is very similar to that observed in crept pure

Al samples [20], where the subgrain size ω can be related to the applied stress (σ) through [21]:

$$\omega = 28b \frac{G}{\sigma}; \quad (1)$$

where G is the shear modulus. Eq. (1) predicts $\omega \approx 8.5 \mu\text{m}$ for an applied stress of 20 MPa at 300°C, in agreement with the present observations where ω is about 7 μm (Fig. 10(a)). For larger precipitates with a mean radius of 7.8 nm (Fig. 10(b)), the dislocations are pinned more efficiently by Al_3Sc precipitates as climbing becomes slower and no dislocation network is observed when the minimum creep rate is reached. The absence of substructure has previously been observed in other coherent precipitation-strengthened alloys, such as Ni-based superalloys [22] or ferritic alloys [23].

4.2. Deformation mechanisms at room temperature

The hardness curves (Figs. 4 and 5) reflect the precipitation process occurring during aging in the two-phase region of the Al(Sc) phase diagram. Our results are comparable with previously published hardness curves for Al(Sc) alloys [2,24]. The average hardness value of our specimens after homogenization and quenching (but before aging) is 215 ± 8 MPa, which is slightly higher than the hardness of pure Al (about 180 MPa [25]), as expected

from the presence of scandium in solid solution. Using the hardness values shown in Fig. 4, and the results presented in our earlier study [3] of precipitate growth during aging of Al-0.3 wt.% Sc alloy, Fig. 11 shows the increase in hardness due to Al₃Sc precipitation as a function of precipitate radius (using as a reference the alloy in its homogenized and quenched state). Because the volume fraction is approximately constant (i.e., ranging from 0.75% at 275°C to 0.71% at 400°C [26]), direct comparison is possible between data points in Fig. 11. Hyland [27] also showed that for an Al-0.25 wt.% Sc alloy, the number density of precipitates starts to decrease at aging times greater than 10,000 s at 288°C and after 2000 s at 343°C. Therefore, to insure that the measurements were performed in the coarsening stage, the data points used in Fig. 11 correspond to aging treatments between 300 and 450°C performed for times longer than 9000 s.

Fig. 11 shows a maximum in hardness increase for radii between 1.5 and 2.0 nm. This result suggests a transition from a shearing mechanism to an Orowan dislocation bypass mechanism, as observed in other systems with shearable, coherent precipitates [28]. The corresponding critical radius can be evaluated using theoretical models [29–31].

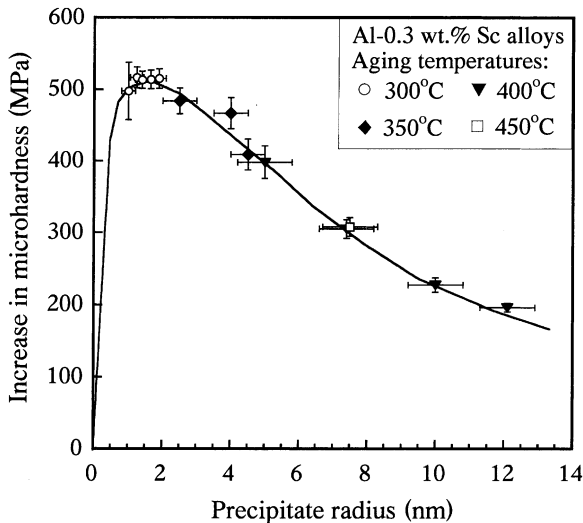


Fig. 11. Increase in ambient temperature microhardness versus precipitate radius for an Al-0.3 wt.% Sc alloy aged at different temperatures.

For the shearing mechanism, the increase in yield strength results from the contributions of order strengthening ($\Delta\sigma_1$), coherency strengthening ($\Delta\sigma_2$), and modulus mismatch strengthening ($\Delta\sigma_3$) [30]. At peak strength, the first contribution is given by:

$$\Delta\sigma_1 = 0.81 M \frac{\gamma_{\text{apb}}}{2b} \left(\frac{3\pi f}{8} \right)^{1/2}; \quad (2)$$

where $M=3.06$ is the mean matrix orientation factor for aluminum [32], $b=0.286$ nm is the magnitude of the matrix Burgers vector [33], f is the volume fraction of Al₃Sc precipitates and $\gamma_{\text{apb}} \approx 0.5$ J/m² is an average value of the Al₃Sc APB energy for the (111) plane taken from several reported values [34–36]. The contribution to the yield strength due to coherency strengthening is expressed by:

$$\Delta\sigma_2 = M\alpha_\epsilon (G\epsilon)^{3/2} \left(\frac{rf}{0.18Gb^2} \right)^{1/2}; \quad (3)$$

where $\alpha_\epsilon = 2.6$ is a constant [30], r is the mean precipitate radius, $G=25.4$ GPa [33] is the shear modulus of Al at room temperature, $\epsilon \approx (2/3)(\Delta a/a)$ is the constrained lattice parameter mismatch, with $\Delta a/a=0.0125$ as the lattice parameter mismatch at room temperature [37]. Finally, strengthening by modulus mismatch is as follows:

$$\Delta\sigma_3 = 0.0055M(\Delta G)^{3/2} \left(\frac{2f}{Gb^2} \right)^{1/2} b \left(\frac{r}{b} \right)^{\frac{3m}{2}-1}; \quad (4)$$

where $\Delta G=42.5$ GPa is the shear modulus mismatch between the matrix and the precipitates [38] and m is a constant taken to be 0.85 [30]. The increase in yield strength due to Orowan dislocation looping is given by Ref. [29] as:

$$\Delta\sigma_{\text{Or}} = M \frac{0.4 Gb}{\pi \sqrt{1-\nu}} \frac{\ln\left(\frac{2r}{b}\right)}{\lambda}; \quad (5)$$

where $\nu=0.34$ is the matrix Poisson's ratio [32] and λ is the inter-precipitate distance, which is taken as the square lattice spacing in parallel planes and is given by Ref. [5] as:

$$\lambda = \left[\left(\frac{3\pi}{4f} \right)^{1/2} - 1.64 \right] r. \quad (6)$$

Fig. 12 shows the theoretical and measured increases in strength as a function of the precipitate size. The volume fraction of Al_3Sc precipitates is taken to be constant (i.e., 0.75%) for calculating the theoretical stresses: the error introduced by this approximation is negligible. Coherency strengthening, $\Delta\sigma_2$, and the modulus mismatch strengthening, $\Delta\sigma_3$, reach maximum values when the shearing dislocation is close to the Al_3Sc interface. However, order strengthening, $\Delta\sigma_1$ is a maximum when the dislocation has sheared half the precipitate. For a given mean precipitate radius, the shearing stress is therefore taken as the highest of the two contributions consisting of order strengthening, $\Delta\sigma_1$ and the sum of the strengthening contributions, $\Delta\sigma_2 + \Delta\sigma_3$, from coherency and modulus mismatch. The data points in Fig. 12 are obtained from the compression yield stress values and hardness measurements using the relationship $\sigma_y \approx \text{HV}/3$, which is satisfactory for aluminum alloys, although it is not valid for pure Al [25]. Good agreement is observed between experimental and theoretical values except near the peak strength, which is over

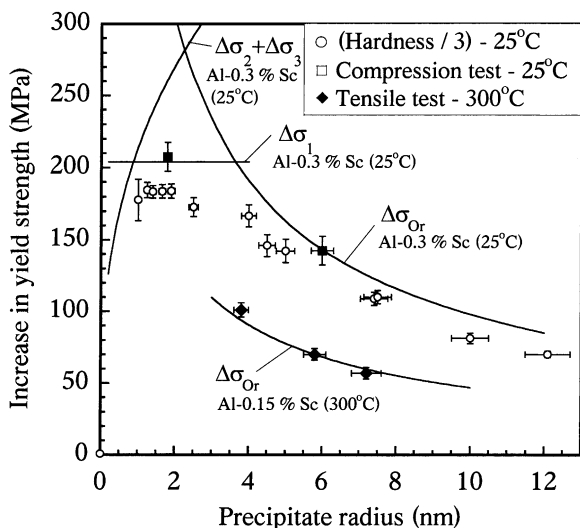


Fig. 12. Increase in yield stress as a function of precipitate radius for an Al-0.3 wt.% Sc alloy aged at different temperatures. Experimental points are obtained from uniaxial yield stress measurements and microhardness measurements (Fig. 11), and the theoretical lines are calculated from Eqs. (1)–(5) for the Orowan stress (σ_{Or}), the cutting stress due to the APB energy ($\Delta\sigma_1$), and the cutting stress due to the lattice and modulus mismatch ($\Delta\sigma_2 + \Delta\sigma_3$).

predicted, probably because of the combined effects of particle shearing and Orowan dislocation bypassing. Near the transition radius, neither of these two mechanisms dominates due to the broad precipitate size distribution (Fig. 2) and the overall yield stress results from a combination of both deformation modes [39]. The critical radius is predicted to be 2.1 nm, in agreement with the observed values of 1.5–2.0 nm. Moreover, as discussed in the previous section, TEM observations of samples deformed at room temperature confirm the operation of the shearing mechanism for small precipitates (1.4 nm) and of the Orowan dislocation looping mechanism for large precipitates (7.8 nm). Specifically, the dislocation spacing in the pairs given by the following equation is in agreement with the estimated value of the APB energy of 0.5 $\text{J}\cdot\text{m}^{-2}$ [29]:

$$l = \frac{Gb}{2\pi(1-\nu)\Delta\sigma_1/M} \quad (7)$$

For an average precipitate radius of 1.4 nm, the dislocation spacing is 12 nm.

4.3. Deformation mechanisms at high temperature

4.3.1. Tensile tests

As anticipated, the yield stress at 300°C for the Al-0.15 wt.% Sc alloy is lower than at room temperature. Using Eq. (5), the decrease of the yield strength due to an Orowan dislocation mechanism with increasing temperature arises from the temperature dependence of the shear modulus, which is given by $\partial G/\partial T = -13.6 \text{ MPa}\cdot\text{K}^{-1}$ for Al [33]. The temperature dependence of the yield stress due to a shearing mechanism results from the temperature dependence of the APB energy, of the shear modulus of the matrix and the precipitate phases, and of the lattice parameter mismatch. Using average thermal expansion coefficient values of $24.7 \cdot 10^{-6} \text{ K}^{-1}$ for Al [40] and $7.5 \cdot 10^{-6} \text{ K}^{-1}$ for Al_3Sc [41], the lattice parameter mismatch is calculated to be $\Delta a/a = 0.0092$ at 300°C. The temperature dependence of the Young's modulus of Al_3Sc is given by $\partial E/\partial T = -26 \text{ MPa}\cdot\text{K}^{-1}$ [42]. The temperature dependence of the APB energy is not known, and is assumed to be negligible. Inserting these

parameters into Eqs. (2)–(6), the transition radius from a shearing mechanism to an Orowan bypass mechanism is calculated to be 2.5 nm at 300°C. The heat-treatments used for the Al-0.15 wt.% Sc alloy produced average precipitate radii ranging from 3.8 to 7.2 nm, and therefore the yield stress should be controlled by the Orowan dislocation mechanism for all samples. As for ambient temperatures, the calculated Orowan yield stress at 300°C is in close agreement with the three experimental values (Fig. 12).

4.3.2. Creep experiments

First, the creep results obtained in the present study are compared to those obtained by Fuller et al. [11]. Their first alloy, containing 0.07 wt.% Sc and aged at 350°C for 1 h, exhibited larger Al₃Sc precipitates than in the present study (estimated to be about 15 nm in radius [3] and most likely with a partial loss of coherency), resulting in a very low number density of precipitates and therefore a weak strengthening effect. Their second alloy, with 0.21 wt.% Sc, and an estimated precipitate radius of 4 nm [3], had a creep strength comparable to the Al-0.2 wt.% Sc alloy of our study.

At low strain rates, the markedly improved creep resistance of the alloys, as compared to pure aluminum (Figs. 6–8), suggests a strong interaction between precipitates and mobile dislocations. The high creep exponents (9–30) in Figs. 6–8 can be interpreted as resulting from a threshold stress, σ_{th} , below which creep rates are negligible. This behavior is described by a modified power-law equation for the strain rate $\dot{\epsilon}$ [43]:

$$\dot{\epsilon} = A \frac{D G b}{k_b T} \left(\frac{\sigma - \sigma_{th}}{G} \right)^n; \quad (8)$$

where A is the Dorn constant, $n=4.4$ is the matrix stress exponent [33], $D = D_0 \exp(-Q/RT)$ is the diffusion coefficient characteristic of the matrix, Q is the diffusion activation energy, k_b is Boltzmann's constant, and σ is the applied stress.

Threshold stress values determined from linear plots of $\dot{\epsilon}^{1/n}$ versus σ are given in Table 2 for the alloys studied. The validity of this approach is illustrated in Fig. 13, where the data fall on straight lines with slopes of 4.5, consistent with the assumed value of 4.4 for the stress exponent. Four

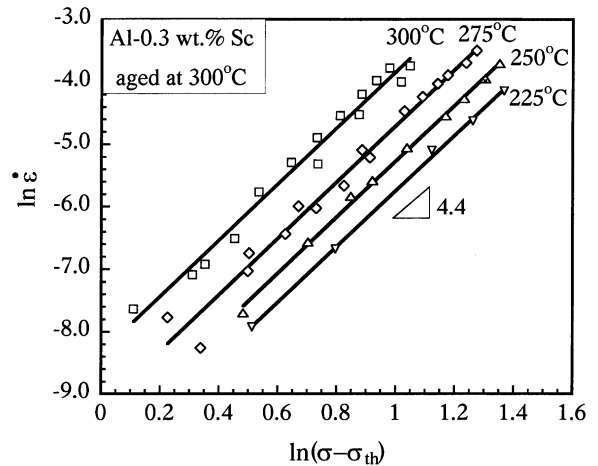


Fig. 13. Ln-ln plot of strain rate versus applied stress minus the threshold stress for the Al-0.3 wt.% Sc alloy data presented in Fig. 7a.

possible mechanisms have been considered to explain the presence of threshold stresses in precipitation- or dispersion-strengthened metals [43]: (a) precipitate shearing; (b) Orowan dislocation looping; (c) dislocations climbing over precipitates; and (d) dislocation detachment from precipitates. The latter mechanism can be jettisoned because it is not active for coherent precipitates [44]. Many creep studies exist in the Ni-Al system, but the coherent γ' -Ni₃Al precipitates are much larger than the present Al₃Sc precipitates. Studying the effect of particle radius distribution on the mechanisms controlling creep of Cu-Cr alloys, with incoherent particles at homologous temperatures T/T_m between 0.5–0.6, Morris and Joye [45], demonstrated that the threshold stress depends on the particle size and therefore on the annealing temperature and time. A dislocation climb mechanism was invoked to explain deformation for an alloy containing intermediate-sized precipitates (about 4.5 nm in radius) and the Orowan mechanism for the largest sizes (about 12 nm in radius). To the best of our knowledge, however, no thorough study on the creep behavior of precipitation-strengthened alloys with coherent, nanometer-size particles without concurrent coarsening has been undertaken. Possible threshold stress mechanisms for Al(Sc) are discussed in the following paragraph.

Values of activation energies can sometimes shed light on the nature of the mechanism controlling the threshold stress. If precipitate shearing is the controlling mechanism, the expected creep activation energy should be similar to that for dislocation creep of single-phase Al_3Sc , (128 kJ mol^{-1} [46]). If dislocation climb, which is diffusion limited in the aluminum matrix, is the rate controlling mechanism, the activation energy should be equal to the value for creep in Al (132 kJ mol^{-1} [33]). Activation energies were obtained from the slope of semi-logarithmic plots of $\dot{\epsilon}$ versus T^{-1} at constant effective applied stress, $\sigma - \sigma_{\text{th}}$. The experimental values for the effective activation energies are $138 \pm 2 \text{ kJ mol}^{-1}$ for Al-0.3 wt.% Sc and $120 \pm 8 \text{ kJ mol}^{-1}$ for Al-0.2 wt.% Sc, calculated at $\sigma - \sigma_{\text{th}} = 4\text{--}15 \text{ MPa}$. The small numerical difference between the experimental values ($129 \pm 8 \text{ kJ mol}^{-1}$) and the theoretical values (128 and 132 kJ mol^{-1}) does not permit to discriminate between the operating mechanism. The shearing mechanism, however, can be excluded since it would lead to yield stress values that are higher by at least one order of magnitude than the observed threshold stresses (Table 1). The Orowan dislocation looping mechanism can be excluded for the same reason, the discrepancy being a factor 2–17 (Table 1). A dislocation climb process is therefore most likely since it operates at stresses lower than the Orowan value, σ_{Or} [47–49].

The threshold stress for climb originates from the increase in dislocation line length as a dislocation climbs over a precipitate. Different values for the threshold stress are predicted depending on the details of the climb geometry. Local climb (where the dislocation line between the precipitates remains in the glide plane) leads to a normalized threshold stress, $\sigma_{\text{th}}/\sigma_{\text{Or}} = 0.4$, independent of the precipitate size. The local climb process model assumes a sharp bend at a precipitate-matrix interface that can be relaxed by diffusion. Thus, general climb models, which are associated with smaller threshold stresses, were developed [43]. The accepted view is that only general climb is possible for coherent precipitates without a detachment stress. In the present case of Al(Sc) alloys, the normalized threshold stress, $\sigma_{\text{th}}/\sigma_{\text{Or}}$, predicted by Rosier and Arzt [49] is independent of the mean precipitate

size and is about 0.03 in the case of the Al-0.3 wt.% Sc alloy. As shown in Fig. 14, however, the experimental values of $\sigma_{\text{th}}/\sigma_{\text{Or}}$ for our Al(Sc) alloys increase from 0.06 to 0.42 as the precipitate radius increases from 1.4 to 9.6 nm. These unexpectedly high experimental values of normalized threshold stress can only be explained if another precipitate-radius dependent mechanism contributes to the threshold stress. A possible mechanism is the repulsive elastic interaction between the matrix dislocations and the coherent precipitates associated with the mismatches in elastic modulus and lattice parameter existing between Al and Al_3Sc . As described in more details in Ref. [1], elastic interactions can significantly contribute to the threshold stress in the Al(Sc) system. Predictions of this model are shown in Fig. 14 and reproduce the experimental trend, i.e. increasing threshold stress with increasing precipitate radius. This model also explains the unexpected results in Fig. 6, where the most creep resistant Al(Sc) alloy has the lowest level of scandium for the same aging condition (300°C, peak aging) and the same testing temperature (300°C). The precipitate radius and thus the threshold stress due to modulus and lattice mismatches are largest for Al-0.1 wt.% Sc. Fig. 14 demonstrates that the threshold stress for the Al-0.1 wt.% Sc alloy is about 40% of the Orowan stress, and is reduced by 4% for the Al-0.3 wt.% Sc alloy. Although the Orowan stress of the Al-0.1 wt.% Sc alloy is lower, the absolute threshold stress value is larger. If Al_3Sc precipitates can remain coherent to large radii (e.g. by reducing the lattice mismatch through alloying), an optimum precipitate size should exist at intermediate radii for a given alloy. This is because the threshold stress in Al(Sc) alloys is a trade-off between the Orowan stress (which decreases with precipitate size) and the repulsive force, due to modulus and lattice mismatches, (which increases with precipitate size).

5. Conclusions

Precipitation strengthening of dilute Al(Sc) alloys with 0.1–0.3 wt.% Sc was studied at ambient and elevated temperatures with the following conclusions:

Table 1
Dependence on the scandium concentration, heat-treatment conditions, precipitate volume fraction, f , average precipitate radius, r , and inter-precipitate spacing, λ , of the experimental threshold stress, σ_{th} , calculated Orowan stress, σ_{or} , and calculated yield stress for a precipitate shearing mechanism, σ_{sh} , all at 300°C

Alloy (wt.% Sc)	Heat-treatment	f^a (%)	r (nm)	λ^b (nm)	σ_{th} (MPa)	σ_{or}^c (MPa)	σ_{sh}^d (MPa)
0.1	275°C, 66h	0.24	4.1	123	8	81	178
0.1	300°C, 24h	0.24	8.5	256	19	47	225
0.2	300°C, 5 h	0.49	3.0	62	14	144	230
0.2	350°C, 5h	0.48	5.0	104	16	100	268
0.2	300°C, 5 h-400°C, 2 h	0.46	5.8	123	22	88	275
0.3	300°C, 5 h	0.75	1.4	23	17	293	224
0.3	350°C, 24 h	0.74	4.8	80	22	130	328
0.3	300°C, 5 h-400°C, 3h	0.71	5.9	101	28	110	344
0.3	300°C, 5 h-400°C, 7 h	0.71	7.8	133	31	89	376
0.3	300°C, 5 h-400°C, 10 h	0.71	9.6	164	32	76	402

^a From lever rule and equilibrium Al(Sc) phase diagram between 300°C and 400°C [26]

^b From Eq. (6)

^c From Eq. (5) (calculated at 300°C)

^d From Eqs. (2)–(4) (calculated at 300°C)

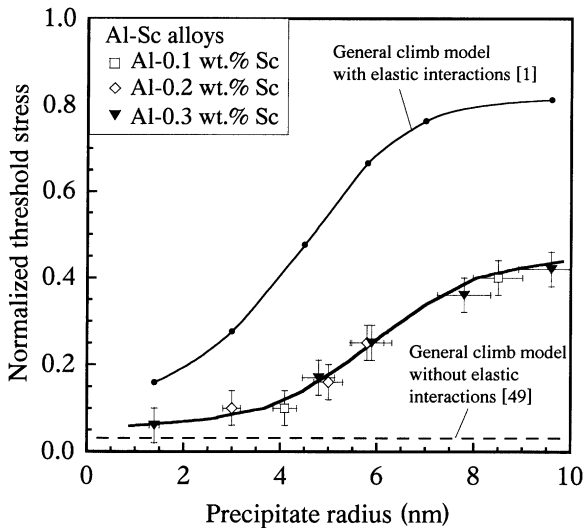


Fig. 14. Normalized creep threshold stress with respect to Orowan stress at 300°C as a function of precipitate radius for an Al-3 wt.% Sc alloy aged at different temperatures. Experimental data is compared to a general climb model without elastic interactions [49] and with elastic interactions [1].

- Heat-treatments at temperatures between 275 and 400°C resulted in coherent, approximately spheroidal $L1_2$ Al_3Sc precipitates with a mean radius between 1.4–9.6 nm (Fig. 1) and with precipitate size distributions close to the Lifshitz-Slyozov-Wagner (LSW) predictions (Fig. 2).
- The time necessary to obtain peak hardness decreases with increasing aging temperature at constant Sc concentration. The decrease in hardness due to coarsening of the Al_3Sc precipitates becomes significant after aging for about 50 h at 350°C or 0.5 h at 400°C (Fig. 4).
- The coherent Al_3Sc precipitates increase the room-temperature flow stress of aluminum significantly, from about 20 MPa for pure Al to 140–200 MPa for Al(Sc) alloys. The precipitate radius corresponding to peak strengthening is about 1.5 nm (Figs. 11 and 12). Quantitative agreement is found with strength values predicted from classical dispersion-strengthening theory, predicting that strength is controlled by a precipitate shearing mechanism for smaller sizes, and the Orowan dislocation bypass mechanism for larger sizes.
- At high temperatures, a creep threshold stress in

the range 8–34 MPa is found for the alloys tested at 300°C (Fig. 7), with an activation energy (measured between 225 and 300°C) of 129 kJ mol^{-1} , which is close to that for creep of pure Al or pure Al_3Sc .

- The threshold stress normalized by the Orowan stress increases monotonically with increasing precipitate size, from 0.06 at 1.4 nm to 0.42 at 9.6 nm (Fig. 14). A general climb model considering the elastic interactions between precipitates and dislocations arising from modulus and lattice mismatches [1] is in semi-quantitative agreement with the experimental threshold stress data (Fig. 14).

Acknowledgements

This research was supported by the United States Department of Energy, Basic Energy Sciences Division, under contracts DE-FG02-98ER45721.

References

- [1] Marquis EA, Dunand DC, accepted for publication, Scripta Materialia, May 2002.
- [2] Toporova LS, Eskin DG, Kharakterova ML, Dobatkina TB. Advanced aluminum alloys containing scandium. Amsterdam: Gordon & Breach, 1998.
- [3] Marquis EA, Seidman DN. Acta Mater 2001;49:1909.
- [4] Drits MY. Phys. Met. Metall 1984;57:118.
- [5] Nembach E. Particle strengthening of metals and alloys. New York, NY: John Wiley, 1997.
- [6] Parker BA. Mat. Sci. Forum 1995;189:347.
- [7] Miura Y, Nakayama M, Furuta A. In: Hosoi Y, Yoshinaga H, Oikawa H, Maruyama K, editors. 7th JIM Int. Symp. on Aspects of High Temperature Deformation and Fracture in Crystalline Materials. Nagoya: The Japan Institute of Metals; 1993. p. 25–5.
- [8] Torma T, Kovacs-Csenty E. J. Mat. Sci. 1989;24:3924.
- [9] Sawtell RR, Jensen CL. Met. Trans, A 1990;21:421–30.
- [10] Nieh TG, Hsiung LM, Wadsworth J, Kaibyshev R. Acta Mater 1998;46:2789.
- [11] Fuller CB, Seidman DN, Dunand DC. Scripta Metall 1999;40:691.
- [12] Wagner C. Z. Elektrochem 1961;65:581.
- [13] Lifshitz IM, Slyozov VV. Phys. Chem. Solids 1961;19:35.
- [14] Ardell AJ. Acta Metall 1972;20:61.
- [15] Sanders TH, Starke Jr EA. Acta Metall 1982;30:927.

- [16] Hatch JE. Aluminum: properties and physical metallurgy. Metals Park, OH: ASM, 1984.
- [17] Novotny GM, Ardell AJ. *Mat Science and Engineering A* 2001;318:144.
- [18] Jha SC, Sanders Jr TH, Dayananda MA. *Acta Metall* 1987;35:473.
- [19] Jeon SM, Park JK. *Phil. Mag* 1994;70:493.
- [20] Martin JL. In: Wilshire B, Evans RW, editors. *Creep of crystalline solids*. Swansea: Unknown; 1985. p. 1.
- [21] Blum W. In: Langdon TG, Merchant HD, Morris JG, Zaidi MA, editors. *Hot deformation of aluminum alloys*. TMS; 1991. p. 18-1.
- [22] Blum W, Reppich B. In: Wilshire B, Evans RW, editors. *Creep behavior of crystalline solids*. Swansea: Pineridge Press; 1985. p. 8-3.
- [23] Zhu SM, Tjong SC, Lai JKL. *Acta Mater* 1998;46:2969.
- [24] Sano N, Hasegawa Y, Hono K. *Supplement to J Physique* 1987;C6:337.
- [25] Tabor D. *The hardness of metals*. New York, NY: Oxford University Press, 1951.
- [26] Jo HH, Fujikawa SI. *Mat. Sci.Eng.* 1993;A171:151.
- [27] Hyland RW. *Metal. Trans. A* 1992;23:1947.
- [28] Jeon SM, Park JK. *Acta Mater* 1996;44:1449.
- [29] Brown LM, Ham RK. In: Kelly A, Nicholson RB, editors. *Strengthening methods in crystals*. Amsterdam: Elsevier; 1971. p. 9–135.
- [30] Ardell AJ. *Met. Trans. A* 1985;16:2131.
- [31] Schleisier C, Nembach E. *Acta metall mater* 1995;43:3983.
- [32] Meyers MA, Chawla KK. *Mechanical metallurgy: principles and applications*. Paramus, NJ: Englewood Cliffs, 1984.
- [33] Frost HJ, Ashby MF. *Deformation mechanism maps*. Oxford: Pergamon Press, 1982.
- [34] Fu CL. *J. Mater. Res* 1990;5:971.
- [35] George EP, Pope DP, Fu CL, Schneibel JH. *ISIJ Intern* 1991;31:1063.
- [36] Fukunaga K, Shouji T, Miura Y. *Mat. Sci.Eng.* 1997;A239:202.
- [37] JCPDS—International Centre for Diffraction Data, v. 2.00, (1998).
- [38] Hyland RW, Stiffler RC. *Scripta Metall. Mater* 1991;25:473.
- [39] Descamps A, Brechet Y. *Acta Mater* 1999;47:293.
- [40] Touloukian YS. *Thermophysical properties of high temperature solid materials*. New York: Macmillan, 1967.
- [41] Harada Y, Dunand DC, unpublished results.
- [42] Drits ME, Toporova LS, Gushchina FL, Fedotov SG. *J. Soviet Non Ferrous Metls. Res* 1984;12:83.
- [43] Cadek J. *Creep in metallic materials*. New York, NY: Elsevier, 1998.
- [44] Srolovitz DJ, Petrovic-Luton RA, Luton MJ. *Acta Mater* 1984;32:1079.
- [45] Morris MA, Joye JC. *Acta Metall. Mater* 1995;43:69.
- [46] Harada Y, Dunand DC. *Acta Mater* 2000;48:3477.
- [47] Shewfelt RS, Brown LM. *Phil. Mag* 1974;30:1135.
- [48] Arzt E, Wilkinson DS. *Acta Metall* 1986;34:1893.
- [49] Rösler J, Arzt E. *Acta Metall* 1988;36:1043.